Numerical Study of Darrieus Wind Turbine Blade Characteristic with Shape Changes of Trailing Edge

Viktus Kolo Koten
Department of Mechanical Engineering, University of Atma Jaya, Makassar, Indonesia
Email: viktus_koten@uajm.ac.id

Syukri Himran, Nasaruddin Salam, and Luther Sule
Department of Mechanical Engineering, University of Hasanuddin, Makassar, Indonesia
Email: syukri_h@yahoo.com, nassalam.unhas@yahoo.co.id, luther.sule@yahoo.co.id

***Abstract*—Performance of the Darrieus turbine is determined by blade characteristics. In the static conditions, an excellent blade characteristic is that it not only has magnitudes such as drag coefficient, lift, and high pressure but also has a distribution of these quantities effectively in each azimuth angle. This study aims to find the right shape of the blade so that the quantities are effectively distributed in various azimuth angles. The formation of the blade model, the establishment of the domain model, element distribution process, determination of boundary conditions, and analysis process of blade characteristics is carried out by CFD. The results of the study show that the blade that changes the shape of the trailing edge of the semicircle is better than the blade that changes the shape of the trailing edge of the triangle and the blade that does not change the shape of the trailing edge**.

***Index Terms*—trailing edge, CFD, blade characteristic**

I. Introduction

Wind turbines are used to convert wind energy into mechanical energy. By the changing wind direction, turbines developed to convert wind energy are Vertical Axis Wind Turbines (VAWT) such as Darrieus, Savonius, and Gorlov turbines. According to A. N. Gorban, A. M. Gorlov and V. M. Silantyev [1], the Darrieus turbine power coefficient is lower than the Gorlov turbine and higher than the Savonius turbine. However, Darrieus turbine construction is easy and feasible to develop further.

Unlike the Savonius, Turbine Darrieus and Gorlov turbines use the National Advisory Committee for Aeronautics (NACA) profile blade. The application of the NACA profile on the Darrieus turbine blade was first carried out by the inventor of the Darrieus turbine. Since it was discovered and patented, the Darrieus turbine has been used as an object of research both to determine the characteristics and to improve turbine performance.

Manuscript received December 1, 2019; revised June 21, 2020.

Studies to improve turbine performance have been carried out in various ways, such as modifying blades, arms, and turbine sizes. Blade modification is done by modifying the overall blade shape, modifying the leading edge, and modifying the trailing edge.

Various researchers have done modification of the trailing edge. H. Beri and Y. Yao [2] modified the trailing edge from rigid to flexible to show better Computational Fluids dynamics (CFD) results than Double Multiple Stream Tube (DMST). S. Y Lin, Y. Y. Lin, C. J. Bai, and W. C. Wang [3] has done modification of other trailing edge. This modification can increase the power coefficient by 2.31 %. In addition to the two trailing edge modification, other modifications have also been made by N. C. Batista, R. Melício, J. C. O. Matias, and J. P. S. Catalão, [4] and F. Ismail and K. Vijayaraghavan [5]. Modifications to the NACA 0018 profile Darrieus turbine blade section conducted by [4] found that the turbine can turn itself at very low wind speeds. However, modifications to the NACA profile blade trailing edge generally only change the profile size. Changing a rigid construction to be flexible on the trailing edge and performed dynamically and statically. Research to determine the characteristics of the NACA profile Darrrieus turbine blade due to changes in the shape of a trailing edge into a semicircle and a triangle has never been done.

This study aims to find the right trailing edge of the blade so that the characteristics of the static blade that are the reference for the performance of the Darrieus turbine can be improved.

Although turbine performance is determined dynamically by turbine characteristics, static turbine characteristics such as drag, lift, and pressure distribution on the blade, an essential role in the process of determining blade shape. Fig. 1 shows a symmetric NACA profile blade construction that turns around the center at point o. When the blade is in quadrant II with an azimuth angle of θ, the blade velocity condition and drag force and lift are shown as illustrated. Relative velocity (w) is obtained from the results of a velocity triangle

doi: 10.18178/ijmerr.9.8.1088-1096

analysis between fluid velocity (V) and blade tangential velocity (u). The direction of the drag force is parallel and in the direction of the relative velocity while the direction of the lift force is perpendicular to the drag force. The direction of the lift force is always perpendicular to the drag force, but the direction of the lift force always changes when rotating through various quadrants. When the blade is in quadrant II, the blade velocity and drag and lift conditions are different from the previous conditions. In quadrant I and III, the lift force tends to pull the blade out of the turbine while in quadrant II and IV, the lift force tends to push the blade to the center of the turbine. The drag force tends to be resistance to blade movement on quadrant I to IV.

The amount of drag force (F_D), lift force (F_L), and pressure can be known through the drag coefficient and lift equations. The magnitude of the drag coefficient (C_D) is the ratio between the drag force on the blade to the flowing fluid force, equation (1). The magnitude of the lift coefficient (C_L) is the ratio between the lift force in the blade to the flowing fluid force, equation (2). The magnitude of the pressure coefficient (C_{pr}) is the ratio between the pressure on the blade to the flowing fluid pressure, equation (3).

$$C_D = \frac{F_D}{\frac{1}{2}\rho A V^2} \quad (1)$$

$$C_L = \frac{F_L}{\frac{1}{2}\rho A V^2} \quad (2)$$

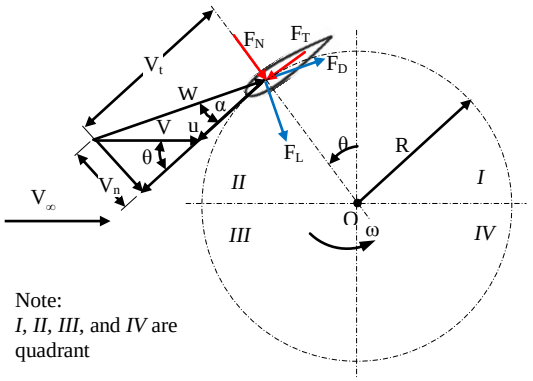

Figure 1. Drag and Lift on the Blade

$$C_{pr} = \frac{P - P_\infty}{\frac{1}{2}\rho V^2} \quad (3)$$

The process of determining C_D and C_L can be done by first knowing the properties of fluid flow. The properties of fluid flow are determined based on the magnitude of the Reynolds number. The magnitude of the Reynolds number in this study is formulated as equation (4),

$$\mathrm{Re} = \frac{\rho V c}{\mu} = \frac{V c}{\upsilon} \quad (4)$$

II. Method

The process of analyzing blade characteristics began with the formation of a blade model, determination of boundary conditions, division of elements, which is done by CFD.

A. Formation of the Blade Model

After conducting a virtual blade formation experiment on the various software, the Autodesk inventor software was selected in this study. The spline command on this software allows the line trajectory not to change position when it passes every specified blade coordinate point. The specified blade coordinates are downloaded from the airfoil tools and modified according to the study boundaries. These coordinate points are connected one by one sequentially to form a NACA 0018 profile turbine blade shown in Fig. 2a. The same coordinate points are connected again and modified according to the semi-circle trailing edge shape like Fig. 2b and the triangular trailing edge shape, as shown in Fig. 2c.

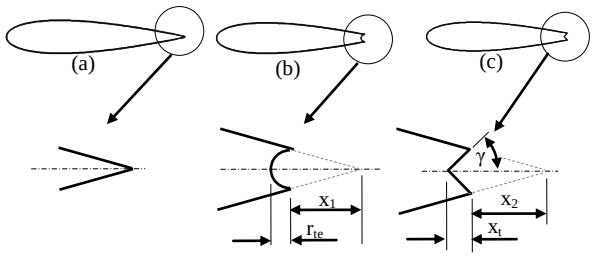

Figure 2. The trailing edge shape of the NACA 0018 profile and its changes. a) Blade shape 1, the blade that does not change the shape of the trailing edge. b) Blade shape 2, the blade that changes the shape of the trailing edge in a half-circle. c) Blade shape 3, the blade that has a triangular trailing edge shape change.

The coordinates of the trailing edge shape changes occur at x = 0.988c or x = 90 mm. Shortening the chord x_1 on blade shape 2 is equal to the shortening of chord x_2 on the blade shape 3. The semicircular radius of (r_{te}) on blade shape 2 is equal to the height of the triangle (x_t) on the blade shape 3. The y-coordinate modified pad x = 90 mm is 2.172 mm for y^+ and -2.172 mm for y^-. Thus the radius of the trailing edge blade that changes is 4.344 mm. The angle formed on the blade that changes the shape of the trailing edge triangle is 2γ or equal to $90^{o,}$ and the height of the triangle is 4.344 mm.

B. Determination of Boundary Conditions and Division of Elements

Azimuth angle (θ) blade is selected in the range from 0^o to 180^o. The Azimuth angle in this range is sufficient to represent the azimuth angle 0^o to 360^o because of the larger azimuth angle; 180^o to 360^o, the results of the study show the same graph pattern.

The domain form is created virtually with Ansys Gambit software. Domain size is determined after

conducting a study of various results of previous studies [3, 5 - 10]. The size of the domain that is too small results in backflow when carrying out an iterative process on CFD. The size of the domain that is too large results in an increase in process time meshing in Gambit, time iteration process in fluent, and requires significant computing power. Fig. 3 shows the shape and size of the domain and the study boundary conditions.

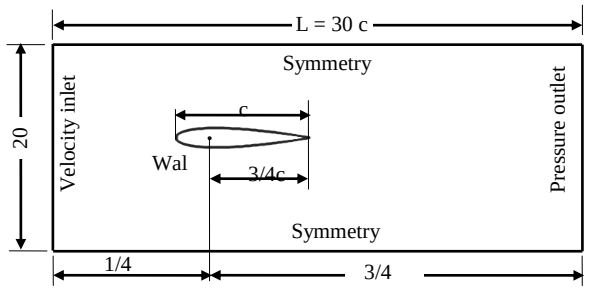

Figure 3. Shape and size of the domain and boundary conditions.

The selection of the type and size of the mesh and the process of making meshing were carried out after studying various literature [2, 5, 6, 8, 11, and 12]. The type of mesh face chosen is tri-pave. Gambit selects the type of mesh that matches the geometry of the object automatically. Gambit does not process the type of mesh chosen if it does not match the geometry of the object. Errors in the mesh formation process result in a large mesh error factor, and the results of the analysis on fluent are incorrect. Mesh size that is too small results in increased processing time in Gambit and requires significant computing power. Mesh size is too large results in the acquisition of less precise results. In this study, the minimum mesh error factor is 0.4388 and a maximum of 0.5374. The magnitude of this mesh error factor is still within reasonable limits because the allowable mesh error factor is 0.8.

The mesh forming process in each blade is shown in Fig. 4a, 4b, 4c, and 4d. All results that have been done on Ansys Gambit and boundary conditions are exported to Ansys Fluent in mesh format.

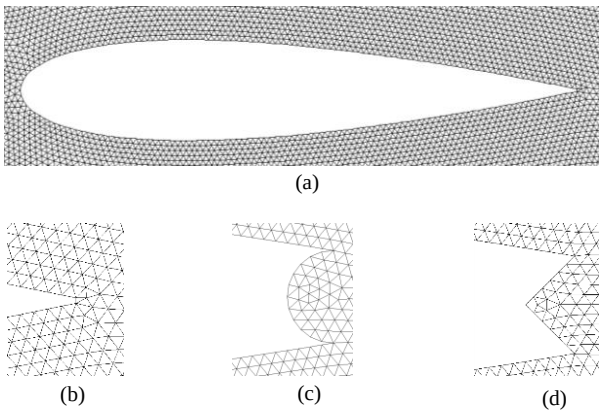

Figure 4. Mesh forming process in each blade. a) The results of the meshing process are bottom-up. b) Mesh on the blade that does not change the shape of the trailing edge. c) Mesh on the blade that changes the shape of the trailing edge in a semicircle. d) Mesh on the blade, which changes the shape of a triangular trailing edge.

The meshing process is carried out bottom-up; the meshing process starts from the mesh line and continues to the mesh face. The space used in the mesh edges is 0.001. The amount of space in the mesh face used is 0.01. The choice of the number of spaces on the mesh edge and mesh face is made by trial and error or following the values listed in Gambit. The trial and error method was chosen in this study because the selection method based on the values stated in the gambit requires a very long time. The incompatibility of spaces in the mesh edge and mesh face causes the mesh to not occur as a whole on the domain. The type of mesh smoothing used is Laplecian L-W. The mesh smoothing command is used to reduce the mesh error factor after the initial mesh process is performed.

C. Analysis of Blade Characteristics

Analysis of blade characteristics was carried out on Ansys Fluent software. This characteristic analysis process consists of grid management and defining models, defining materials and determining boundary conditions, iterating processes, and post-processing. All of the characteristics of this study are carried out by double-precision (2ddp) in two dimensions (2D).

Grid management and models defining. Grid management is done to adjust the number of elements, domain size, analysis coordinate points, and size scale read on Fluent with those made in Gambit. Defining the model is done by first calculating the Reynolds number. Based on equation (4), the magnitude of the Reynolds number in this study is 4.45×10^4. Fluent provides several models of analysis for various cases based on the magnitude of the Reynolds number. This study uses the standard k-ε analysis model because the calculation of Reynolds numbers shows that the type of flow is turbulent. The use of this analysis model was chosen after a study of the various results of previous studies [2, 13, and 14]. Although the study on [15- 18] used the k-ω SST analysis model, the selection of k-ε standard was carried out only to see blade characteristics in different trailing edge shapes. The selection of an incompatible and different analytical model on each blade trailing edge shape produces incorrect blade characteristics and does not converge in the iteration process.

Material defining and boundary conditions. The material used in this study is air with a temperature of 300 K. Although Fluent has prepared fluid properties by default, fluid properties are inputted again based on fluid temperature. The velocity of fluid flow in the inlet velocity is 7.5 m/s, and the channel cross-sectional area is 1 m^2. The depth of the domain is obtained after dividing the area by 1 m^2 with the width of the domain, which is the boundary of the study. The depth of the domain in Fig. 3 is 0.5 m.

Iteration process. This process begins by re-ascertaining the incoming airspeed of 7.5 m/s. The selection of check convergence values in this study has been compared with studies [9, 19, and 20]. The choice of check convergence that is too large results in incorrect blade characteristics. The check convergence value is selected on a large number and then gradually reduced to

produce blade characteristics that do not change again. The selected value of convergence is 1 x 10^{-5}. If the check convergence value is reduced again, it will produce the same or unchanged blade characteristics. It indicates that the selected check convergence value is correct. The reference value is selected on the velocity inlet and reference zone on the air. Blade characteristics such as C_D, C_L, C_{pr}, and pressure distribution are shown in parts that are treated as wall (blade) and which are fluidized.

The selection of an improper wall in a Gambit operation can produce blade characteristics that are erroneous in the fluent process. In this study, only the blade is treated as a wall, while the treatment in other parts is shown in Fig. 3. The prediction of the number of iterations performed is entered first into Fluent. The iteration process is stopped even though the number of iterations entered has not been reached. This termination indicates that the iteration process has reached a convergence calculation; the results sought have been obtained. If the number of iterations entered does not occur convergence when the operation, then the fluent automatically asks for the addition of the number of iterations.

Post Processing. This process is the final stage of the research method. This process is needed to see counters and speed vectors, counters and pressure vectors, pressure distribution curves, and other essential things.

III. Result and Discussion

The shape changes on the trailing edge blade produce different blade characteristics. Fig. 5, 6, and 7 show successively azimuth angle $v_{s.}$ drag coefficient graphs, azimuth angle $v_{s.}$ lift coefficient, and azimuth angle $v_{s.}$ pressure coefficient graph. The force of fluid flowing in the domain is the same in various azimuth angles. The lift and drag styles and pressures change with each azimuth angle position. Changes in drag and lift forces, and this pressure are affected by changes in the cross-section of the blade and the length of the chord that is exposed to the fluid at various azimuth angles. Changes in the lift force, drag force, and pressure cause the drag coefficient lift, and pressure to change.

A. Drag Coefficient

Based on Fig. 1, the direction of the drag force is always in line with the relative velocity. The relative velocity formed is a combination of fluid velocity v with the tangential velocity u. Equation (1) defines the drag coefficient is proportional to the drag force that occurs in the blade. Drag force is a barrier force that is avoided or minimized. Fig. 1 shows the drag force can be broken down into two directions; perpendicular and parallel to the radius of the turbine. The drag force that is perpendicular to the turbine radius always blocks the movement of the blade. The drag force that is parallel to the turbine radius can push the blade towards the shaft and pull the blade away from the turbine shaft. Drag forces push the blade when the blade is in quadrants *II* and *IV*. The drag force pulls the blade when the blade is on *I* and *III*. This cycle of changes continues as long as the blade moves around the turbine shaft.

Overall, a more significant drag occurs in the blade that does not change the shape of the trailing edge (blade shape 1). In this condition, blade shape 1 has a chord size that is longer than blade shape 2 and blade shape 3. The blade that has a longer, larger chord absorbs fluid force than a blade that has a shorter chord.

In azimuth angle 180^o, blade shape 1 has a smaller drag than blade shape 2 and blade shape 3. This condition is influenced by the cross-sectional area of the blade, which is perpendicular to the direction of fluid flow. In the azimuth angle 180^o, the cross-sectional area of blade shape 1 is smaller than the cross-sectional area of blade shape 2 and blade shape 3. In the larger cross-sectional area, the blade absorbs more fluid force than the smaller cross-sectional area. Specifically, on blades that were trailing edge shape changes, blade shape 2 has a drag coefficient higher than blade shape 3. A comparison of these coefficients can be made because the blade has the same shortening chord. The results of the study show that blade shape 2 and blade shape 3 have the same blade characteristics.

In the azimuth angle 180^o, the angle of attack coincides with the chord so that the angle of attack becomes 0^o. In addition to coinciding with the chord, the angle of attack also coincides with the azimuth angle. The overlapping angle of attack and azimuth angle has been proven by researchers [5, 22, and 23]. In this azimuth angle, the largest drag coefficient occurs consecutively, starting from blade shape 2, blade shape 3, and blade shape 1. The drag coefficient difference between blade shape 2 with blade shape 3 and blade shape 1 is 0.66 % and 26.88 %. The drag coefficient on blade shape 2 is 0.66 % greater than blade shape 3 and 26.88 % of blade shape 1. The magnitude of this difference indicates that blade shape 2 is better than blade shape 3 and blade shape 1.

Just like in the azimuth angle 180^o, the angle of attack also coincides with the chord in the azimuth angle 0^o. The largest drag coefficient on azimuth angle 0^o occurs in succession on blade shape 2, blade shape 3, and blade shape 1. The difference in drag coefficient between blades shape 2 with blades shape 3 and 1 is 0.41 % and 3.58 %, respectively. The drag coefficient on blade shape 2 is smaller than 0.41% of blade shape 3 and 3.58% of blade shape 1. The difference in drag at the azimuth angle is so small that it is assumed to be the same.

In the azimuth angle range of 30^o to 150^o, the smallest drag coefficient occurs at 150^o azimuth angle for all blade shapes. The smallest drag coefficient on azimuth angle 150^o occurs on the blade shape 3, blade shape 2, and blade shape 1, respectively. Differences in drag coefficient between blade shape 1 with blade shape 2 and blade shape 3 are 6.93 % and 6.34 %, respectively. The drag coefficient on blade shape 1 is 6.93 % smaller than blade shape 2 and 6.34 % of blade shape 3. The drag coefficient difference between blade shape 2 and blade shape 3 is 0.62%. The small percentage difference in drag coefficient on blade shape 2 with blade shape 3 shows

that the difference is not significant or assumed to be the same.

In the range of azimuth angle 30° to 150°, the largest drag coefficient occurs in the azimuth angle 90°. The results of the study showed that in the azimuth angle 90°, the largest drag coefficients occurred respectively in blades 1, 2, and 3. The drag coefficient differences between blade shape 1 and blade shape 2 and blade shape 3 were 11.23 % and 11, 37 %, respectively. The drag coefficient on blade shape 1 is 11.23 % smaller than blade shape 2 and 11.37% of blade shape 3. The difference in drag coefficient between blade shape 2 and blade shape 3 is 0.15%. The small percentage difference in drag coefficient on blade shape 2 with blade shape 3 shows that the difference is not significant or assumed to be the same.

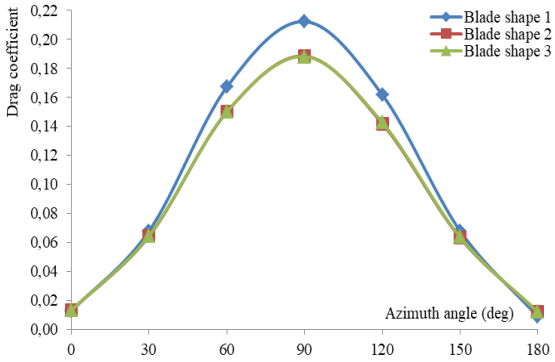

Figure 5. Azimuth angle vs. drag coefficient.

B. *Lift Coefficient*

Equation (2) defines the lift coefficient as directly proportional to the lift force on the blade. The lift force on the Darrieus turbine blade is a force that can enlarge or reduce tangential forces and normal forces, as shown in Fig. 1. Tangential force is a force whose direction is perpendicular to the turbine radius, while the normal force is a force that is in the direction of the turbine radius.

The application of the lift force on the Darrieus turbine can be marked as positive or negative. The positive lift force indicates that the blade experiences an outward turbine force while the negative lift force indicates that the blade is under pressure into the turbine. Changes in the direction of the lift force indicate that under certain conditions, the lift force can enlarge and reduce the tangential force and normal force.

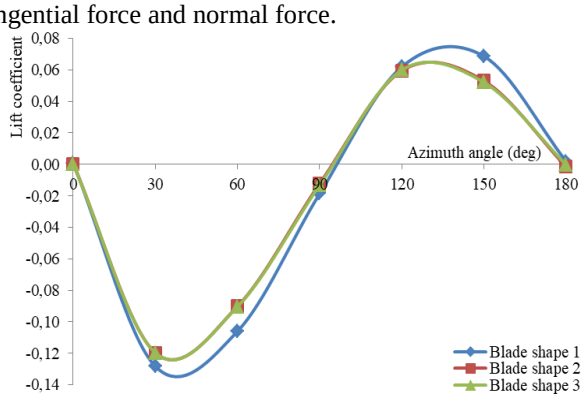

Figure 6. Azimuth angle vs. lift coefficient

Overall, a higher lift coefficient occurs in the blade that does not change the shape of the trailing edge (blade shape 1). In this condition, the blade shape 1 has a chord size longer than the blade shape 2 and blade shape 3. Blades that have extended chords absorb more fluid forces than blades that have shorter chords. Blade with a longer blade trailing edge provides tangential force to a larger turbine shaft.

Conversely, a blade with a shorter blade trailing edge can reduce tangential force to the turbine shaft. Blade with a longer blade trailing edge provides normal force to the larger turbine shaft. Conversely, a blade with a shorter blade trailing edge reduces the normal force to the turbine shaft.

Blade shape 1, blade shape 2, and blade shape 3 have very small lift coefficients on the azimuth angle 0° and 180°. In azimuth 0°, the biggest lift occurs in succession on blade shape 1, blade shape 2, and blade shape 3. In azimuth angle 180°, the largest lift occurs in succession on blade shape 1, blade shape 2, and blade shape 3. Besides experiencing different coefficients lift, the direction of lift force at the blade shape 2 and blade shape 3 also experience differences with blade shape 1. Thus a negative sign on the lift coefficient at the blade shape 2 and blade shape 3 indicates that the fluid is pressing the blade. The difference in the lift coefficient on azimuth angle 0° and 180° is not seen in Fig. 6. Because of the small difference in the lift coefficient on the azimuth angle 0° and 180°, the lift coefficient in this azimuth angle is assumed to be the same.

When the blade rotates around the shaft, the blade passes through four quadrants alternately, as shown in Fig. 1. This blade rotation causes the lift coefficient on the blade to change the sign from positive to negative and vice versa. This change produces the lift coefficient to zero at a specific position. Because the lift coefficient value depends on the flowing fluid force and the lift force that strikes the blade, the value of the zero-lift is affected by the absence of a lift force that hits the blade. Conclusions about the absence of a lift force are also mathematically proven. The coefficient of the lift to zero in blade shape 1 occurs in the azimuth angle 96.92°. The lift coefficient value becomes zero at the blade shape 2 and blades shape 3 occurring consecutively at azimuth angle 95.11° and 95.39°. The zero-lift force is very good at the Darrieus turbine because it does not add normal force to the turbine shaft.

Blade shape 2 has a lift coefficient greater than blade blades shape 3. This coefficient comparison can be made because the blade experiences the same chord shortening ($x_1 = x_2$) and the same trailing edge change depth ($r_{tb} = x_t$). Explanation of $x_1 = x_2$ and $r_{tb} = x_t$ is shown in Fig. 2. The diameter of the circle on the trailing edge of the blade that changes shape is determined based on the third point of the trailing edge. This point is also a reference to changes in the triangle trailing edge.

When the blade is in quadrant *II*, the smallest coefficient of lift occurs in the azimuth angle 38° for blades shape 1 and 36° for blade shape 2 and blade shape 3. In the azimuth angle 38°, the smallest lift coefficient

that occurs is -0.1313 at the blade shape 1. In azimuth angle 36°, the smallest lift coefficient that occurs is -0.1231 at the blade shape 2 and blade shape 3. This last condition shows that the coefficient of the lift does not change for blade shape 2 and blade shape 3 in the azimuth angle 36°, so it is assumed to be the same.

When the blade is in quadrant *III*, the largest lift coefficient occurs at 138° azimuth angle for blades shape 1 and 129° for blade shape 2 and blade shape 3. The largest lift coefficient that occurs at 138° azimuth angle is 0.0695 on blade shape 1. The largest lift coefficient that occurs at azimuth angle 129° is 0.0612 on blade shape 3 and 0.0607 on blade shape 2. Especially in azimuth angle 38° where the maximum lift coefficient on blade shape 2 and 3 occurs, the coefficient of lift on blade shape 3 is 0.75% smaller than blade shape 2. Condition this shows that the difference in the lift coefficient on blade shape 2 and blade shape 3 is so small that it can be assumed to be the same.

C. Coefficient and Pressure Distribution

Fig. 7 shows a graph of the pressure coefficient. Although it has different coefficient values, the pressure coefficient chart pattern is the same as the drag coefficient chart pattern. Therefore, the discussion in this section is the same as discussing the drag coefficient.

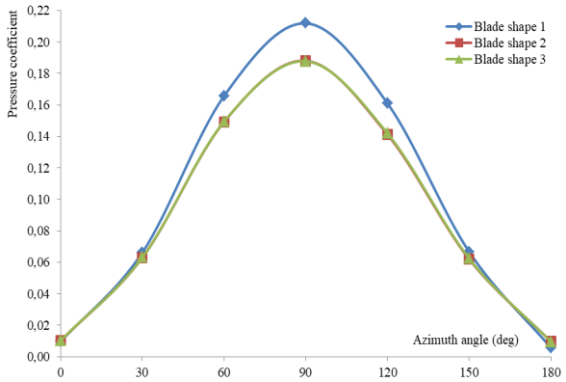

Figure 7. Azimuth angle Vs pressure coefficient.

Fig. 8 shows the distribution of pressure on the azimuth angle 0°. Fig. 8a, 8b, and 8c show the pressure distribution for the entire blade. Maximum pressure occurs at the leading edge, and minimum pressure occurs on the upper and lower sides of the blade. The pressure distribution on the trailing edge in all three blades is shown in Fig. 8d, 8e, and 8f. Due to changes in the shape of the trailing edge blade results in a change in pressure distribution on the trailing edge blade. Trailing edge shaped blades such as Fig. 8e and 8f experience the effect of vortex pressure on the trailing edge blade. Vortex effect on trailing edge blade causes an increase in pressure coefficient. Increasing the pressure coefficient value can inhibit the forward movement of the blade as shown in Fig. 1.

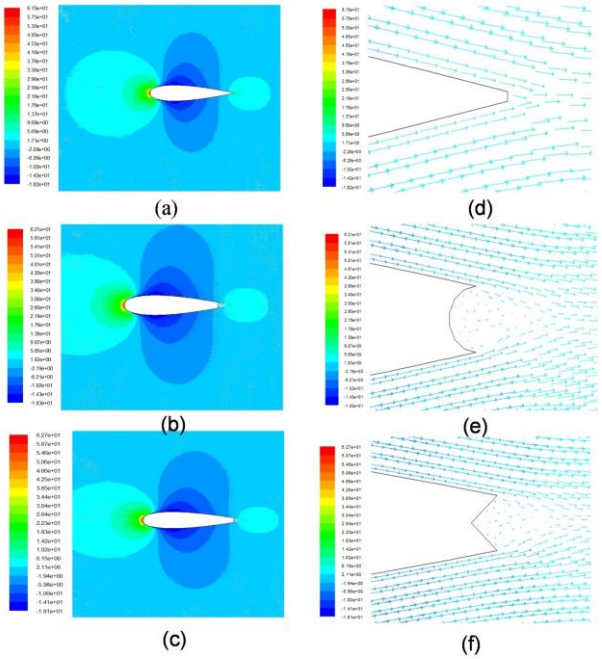

Figure 8. Pressure distribution in azimuth angle 0°. (a) Pressure distribution on blade shape 1, (b) blade shape 2, (c) blade shape 3. (d) Pressure distribution on trailing edge blade shape 1, (e) blade shape 2, (f) blade shape 3.

Fig. 9 shows the distribution of pressure in azimuth angle 180°. Fig. 9a, 9b, and 9c show the pressure distribution for the entire blade. Maximum pressure occurs on the trailing edge, and minimum pressure occurs on the upper and lower sides of the blade.

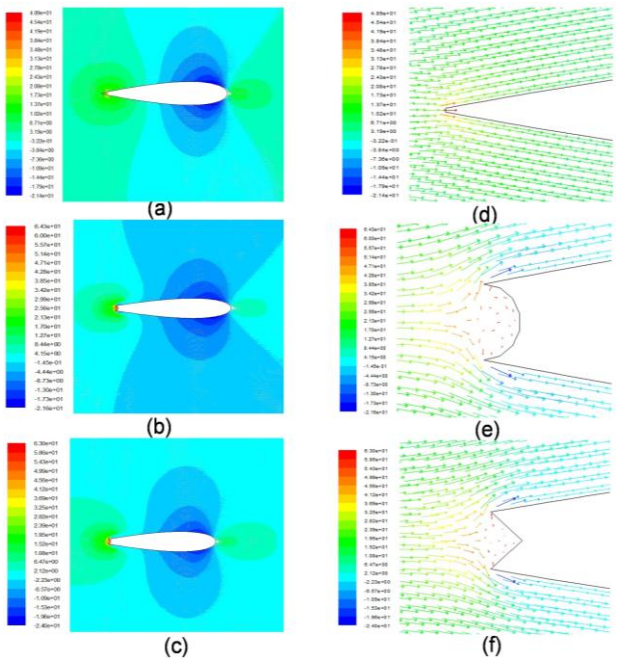

Figure 9. Pressure distribution in azimuth angle 180°. (a) Pressure distribution on blade shape 1, (b) blade shape 2, (c) blade shape 3. (d) Pressure distribution on trailing edge blade shape 1, (e) blade shape 2, (f) blade shape 3.

The pressure distribution on the trailing edge is shown in Fig. 9d, 9e, and 9f. As a result of the blade trailing edge changes produce changes in pressure distribution on

the blade trailing edge. Trailing edge shaped blades such as Fig. 9e and 9f experience the effect of vortex pressure on the blade trailing edge. Vortex effect on blade trailing edge can increase the pressure coefficient value.

Fig. 10 shows the distribution of pressure at azimuth angle 90^o. Fig. 10a, 10b, and 10c show the pressure distribution for the entire blade. The maximum pressure occurs in the upper surface facing the inlet velocity, but the minimum pressure does not occur on the lower surface. Minimum pressure occurs at the leading edge. The pressure distribution on the trailing edge in the three blades is shown in Fig. 10d, 10e, and 10f. Unlike blade shape 1, changes at the blade shape 2 and blade shape 3 trailing edge result in changes in pressure distribution on the blade trailing edge. Trailing edge shaped blades such as Fig. 10e and 10f undergo pressure vortex on the trailing edge. Apart from the chord shortening, the effect of vortex pressure on the trailing edge can reduce the pressure coefficient. Decreasing the pressure coefficient on the azimuth angle can inhibit the forward movement of the blade concerning Fig. 1.

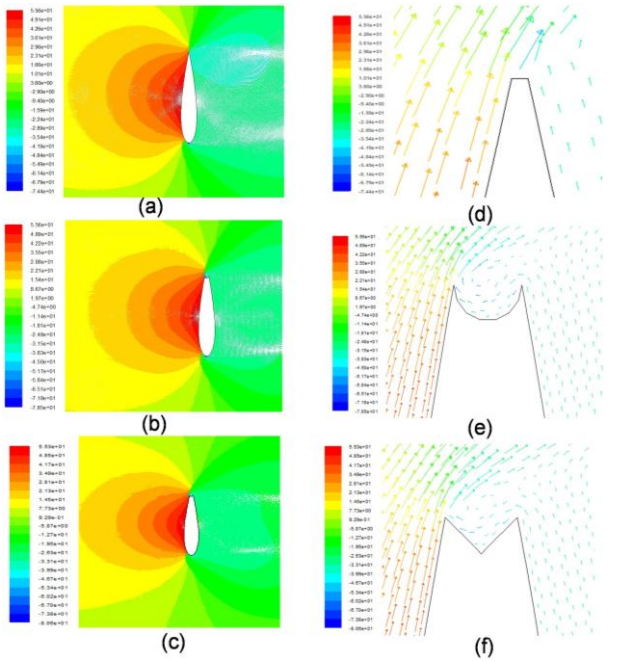

Figure 10. Pressure distribution in azimuth angle 90^o. (a) Pressure distribution on blade shape 1, (b) blade shape 2, (c) blade shape 3. (d) Pressure distribution on trailing edge blade shape 1, (e) blade shape 2, (f) blade shape 3.

Fig. 11 shows the pressure distribution in the azimuth angle 30^o, 60^o, 120^o, and 150^o. The pattern of distribution of pressure on the blade trailing edge is the same as the pattern of pressure distribution in the azimuth angle 0^o and 90^o. Just like the azimuth angle 0^o and 90^o, the vortex pressure that occurs on the trailing edge of the blade that changes trailing edge shape results in a decrease in the pressure coefficient. While the pressure vortex on the blade trailing edge, which changes shape in the azimuth angle above 165^o to 180^o, can increase the pressure coefficient.

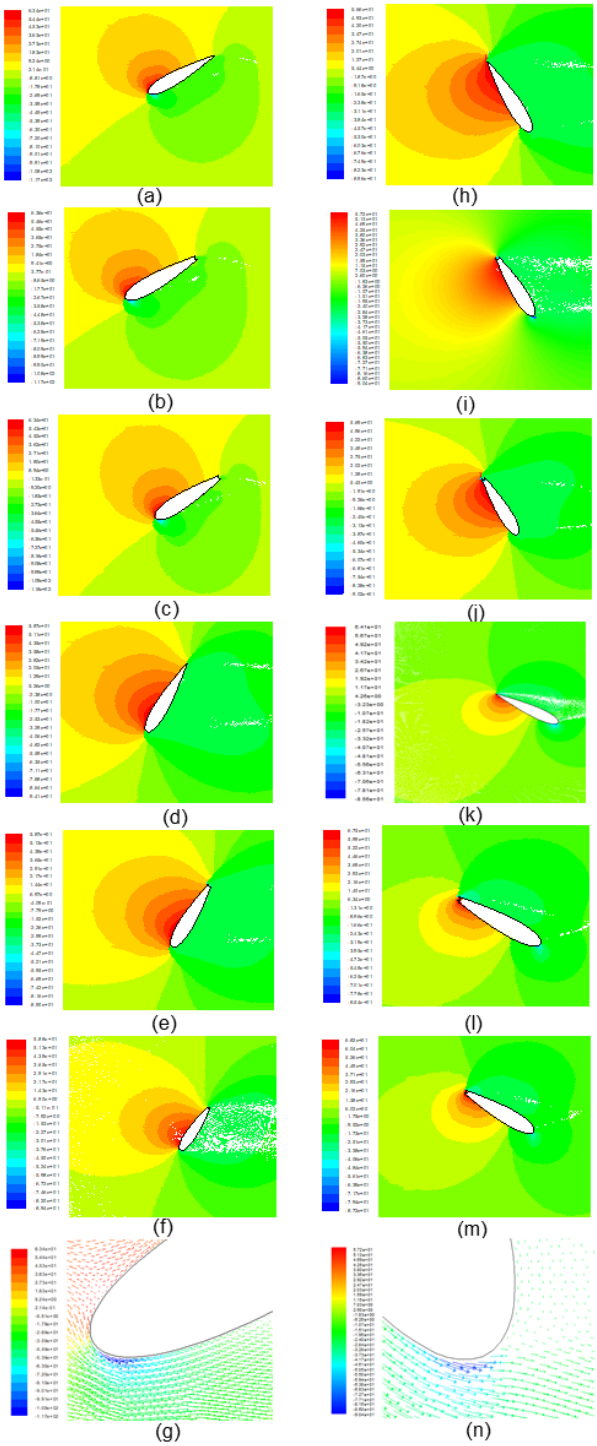

Figure 11. (a) Pressure distribution on azimuth angle 30^o in blade shape 1, (b) blade shape 2, (c) blade shape 3. (d) Pressure distribution on azimuth angle 60^o in blade shape 1, (e) blade shape 2, (f) blade shape 3. (g) Pressure distribution at the leading edge on azimuth angle 30^o. (h) Pressure distribution on azimuth angle 120^o on blade shape 1, (i) blade shape 2, (j) blade shape 3. (k) Pressure distribution on azimuth angle 150^o on blade shape 1, (l) blade shape 2, (m) blade shape 3. (n) Pressure distribution at the leading edge on azimuth angle 120^o.

The difference in pressure distribution on the trailing edge between blade shape 1 with blade shape 2 and blade shape 3 is very significant. At the trailing edge blade shape 1 does not experience pressure vortex while at the blade shape 2 and blade shape 3 always experiences

pressure vortex. Although the difference in pressure distribution on blade shape 2 and blade shape is minimal, blade shape 2 has a pressure coefficient higher than that of blade shape 3 in the azimuth angle 165° to 180°.

The biggest pressure always occurs in part facing the velocity inlet, but the smallest pressure does not occur in part facing the pressure outlet. The smallest pressure always occurs at the leading edge as shown in Fig. 11g and 11n. This Fig. 11g and 11n represent the overall condition of the pressure distribution at the leading edge of the azimuth angle 30°, 60°, 90°, 120°, and 150°.

In conjunction with Fig. 1, these results show that in addition to 0° and 180° azimuth angles, the blade always moves towards the leading edge or rotates around the axis of the axis with angular velocity ω. Even though the number of blades only one cannot be done because, in the azimuth angle 0°, the blade cannot move anymore. The minimum pressure does not occur at the leading edge.

IV. Conclusion

Based on the results of the study, it can be concluded that the best drag distribution occurs in the blade that undergoes trailing edge shape changes. It is known through the drag coefficient distribution that occurs in the azimuth angle 165° - 180°. The drag coefficient on the blade that undergoes trailing edge changes is higher than the blade that does not change the shape of the trailing edge. Although the difference in drag coefficient between blades that change the shape of a semicircular trailing edge with a blade that changes the shape of the trailing edge of a triangle is very small, the results of the study show that the blade with a semicircular trailing edge is better than a blade with a triangular trailing edge shape.

Conflict of Interest

This study was conducted without any cost or conflict of interest from any party. The equipment used in this study was prepared by Hasanuddin University Makassar.

Author Contributions

The first author search references prepare research data, collects studies, and sends the results of studies to a mutually agreed journal. The second author analyzes the drag data. The third author analyzes elevator data. The fourth author analyzes the pressure distribution data.

Acknowledgment

Thank the leadership and staff of the fluid mechanics laboratory who have prepared the research equipment.

References

[1] A. N. Gorban, A. M. Gorlov, and V. M. Silantyev, "Limits of the Turbine Efficiency for Free Fluid Flow," *Journal of Energy Resources Technology, vol. 123, pp. 311–317, 2016*.

[2] H. Beri and Y. Yao, "Double Multiple Stream Tube Model and Numerical Analysis of Vertical Axis Wind Turbine," *Energy and Power Engineering, vol. 2011, July, pp. 262–270, 2011.*

[3] S. Y. Lin, Y. Y. Lin, C. J. Bai, and W. C. Wang, "Performance analysis of vertical-axis-wind-turbine blade with modified trailing edge through computational fluid dynamics," *Renew. Energy, vol. 99, pp. 654–662, 2016.*

[4] N. C. Batista, R. Melício, J. C. O. Matias, and J. P. S. Catalão, "New blade profile for Darrieus wind turbines capable to self-start." *IET Conference on renewable power generation, Lisbon, 6-8 September, 2011.*

[5] F. Ismail and K. Vijayaraghavan, "The effects of aerofoil profile modification on a vertical axis wind turbine performance," *Energy, vol. 80, pp. 20–31, 2015*.

[6] N. Salam, R. Tarakka, and R. Bachmid, "The effect of the addition of inlet disturbance body (IDB) to flow resistance through the square cylinders arranged in tandem," *International Review of Mechanical Engineering, vol. 11, no. March, pp. 181–190, 2017.*

[7] Z. Xingwei, "Numerical study on effect of leading-edge tubercles," *Aircraft Engineering and Aerospace Technology, vol. 4, pp. 247–257, 2013.*

[8] P. W. Weber and M. M. Murray, "Numerical Study of Aerodynamic Characteristics of a Symmetric NACA Section with Simulated Ice Shapes," *Journal of Physics, 2016.*

[9] M. Raciti Castelli, A. Englaro, and E. Benini, "The Darrieus wind turbine: Proposal for a new performance prediction model based on CFD," *Energy, vol. 36, no. 8, pp. 4919–4934, 201*1.

[10] A. Rezaeiha, I. Kalkman, and B. Blocken, "Effect of pitch angle on power performance and aerodynamics of a vertical axis wind turbine," *Appl. Energy*, vol. 197, pp. 132–150, 2017.

[11] C. Bak and P. Fuglsang, "Modification of the NACA 632-415 Leading edge for better," *Journal of Solar Energy Engineering, vol. 124, no. November, pp. 327–334, 2002*.

[12] M. H. Mohamed, A. M. Ali, and A. A. Hafiz, "CFD analysis for H-rotor Darrieus turbine as a low speed wind energy converter," *Eng. Sci. Technol. an Int. J.*, vol. 18, no. 1, pp. 1–13, 2015.

[13] R. Gosselin, G. Dumas, and M. Boudreau, "Parametric study of H-Darrieus vertical-axis turbines using uRANS simulations," 21st *Annual Conference of the CFD Society of Canada, Sherbrooke, Canada, May 6–9, 2013.*

[14] C. Stouta, S. Islama, A. Whitea, S. Arnotta, E. Kollovozia, and Morven, "Efficiency Improvement of Vertical Axis Wind Turbines with an Upstream Deflector," *2nd International Conference on Advances on Clean Energy Research, ICACER, 7-9 April, Berlin, Germany, vol. 118, pp. 141-148, 2017.*

[15] A. Tummala, R. Kishore, D. Kumar, V. Indraja, and V. H. Krishna, "A review on small scale wind turbines," *Renew. Sustain. Energy Rev., vol. 56, pp. 1351–1371, 2016.*

[16] E. Amet, T. Maître, C. Pellone, and J.-L. Achard, "2D Numerical simulations of blade-vortex interaction in a Darrieus turbine," *J. Fluids Eng., vol. 131, no. 11, pp. 1-15, 2009.*

[17] P. Marsh, D. Ranmuthugala, I. Penesis, and G. Thomas, "Three dimensional numerical simulations of a straight-bladed vertical axis tidal turbine," *8th Australasian Fluid Mechanics Conference Launceston, 3-7 December, pp. 2–5, 2012.*

[18] Y. Yan, E. Avital, J. Williams, and T. Korakianitis, "CFD Analysis for the Performance of Gurney Flap on Aerofoil and Vertical Axis Turbine", *International Journal of Mechanical Engineering and Robotics Research Vol. 8, No. 3, May, pp 385-392. 2019.*

[19] S. Becz, M. S. Majewski, and L. S. Langston, "Leading edge modification effects on turbine Cascade endwall loss," *Proceedings of ASME Turbo Expo 2003 Power for Land, Sea, and Air, June 16–19, Atlanta, Georgia, USA, pp. 1–9, 2003.*

[20] A. Rezaeiha, I. Kalkman, and B. Blocken, "CFD simulation of a vertical axis wind turbine operating at a moderate tip speed ratio : Guidelines for minimum domain size and azimuthal increment," *Renew. Energy, vol. 107, pp. 373–385, 2017.*

[21] A. Rezaeiha, I. Kalkman, H. Montazeri, and B. Blocken, "Effect of the shaft on the aerodynamic performance of urban vertical axis wind turbines," Energy Convers. Manag., vol. 149, no. July, pp. 616–630, 2017.

[22] S. Halle and I. Paraschivolu, "Numerical simulation of dynamic stall around an airfoil in Darrieus motion," *Journal of Solar Energy Engineering, vol. 121, no, pp 69-76, 1999.*

[23] A. O. Onol and S. Yesilyurt, "Effects of wind gusts on a vertical axis wind turbine with high solidity," *Jnl. Wind Eng. Ind. Aerodyn.*, vol. 162, no. June 2016, pp. 1–11, 2017.

Viktus Kolo Koten – born in Lewo Bao on June 15th, 1975, is the student S3 in the Department of Mechanical Engineering, Faculty of Engineering, Hasanuddin University Makassar Indonesia. He holds a magister degree from the Department of Mechanical Engineering, Faculty of Engineering, Hasanuddin University Makassar Indonesia. His research fields include fluid machines, particularly on blade and wind turbines.

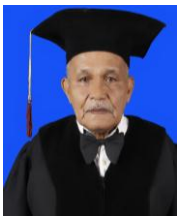

Syukri Himran – born in Gorontalo on September 27th, 1942, is Professor emeritus and the Chairman of Fluid Mechanics Laboratory in Department of Mechanical Engineering, Faculty of Engineering, Hasanuddin University Makassar Indonesia. He holds a doctoral degree from Institut Teknologi Bandung, Indonesia. His research fields include fluid dynamics and energy.

Nasaruddin Salam – born in Bulukumba on December 20th, 1959, is the Professor and the Chairman of the Fluid Mechanics Laboratory in the Department of Mechanical Engineering, Faculty of Engineering, Hasanuddin University Makassar Indonesia. He holds a doctoral degree from Brawijaya University, Malang Indonesia. His research fields include fluid dynamics, particularly on tandem bodies. Prof. Nasaruddin is a member of the Institutions of Engineers Indonesia.

Luther Sule – born in Tana Toraja on August 27th, 1956, is an Associate Professor and the Chairman of Fluid Machine Laboratory in the Department of Mechanical Engineering, Faculty of Engineering, Hasanuddin University Makassar Indonesia. He holds a doctoral degree from Brawijaya University, Malang Indonesia. His research fields include a water turbine.